Precise determination of phonon constants in lead-free monoclinic $(K_{0.5}Na_{0.5})NbO_3$ single crystals

Muhammad Asif Rafiq, Peter Supancic, M. Elisabete Costa, Paula M. Vilarinho, and Marco Deluca'

Citation: Appl. Phys. Lett. **104**, 011902 (2014); doi: 10.1063/1.4860416
View online: http://dx.doi.org/10.1063/1.4860416
View Table of Contents: http://aip.scitation.org/toc/apl/104/1
Published by the American Institute of Physics

Precise determination of phonon constants in lead-free monoclinic $(K_{0.5}Na_{0.5})NbO_3$ single crystals

Muhammad Asif Rafiq,[1] Peter Supancic,[2] M. Elisabete Costa,[1] Paula M. Vilarinho,[1] and Marco Deluca[2,3,a)]

[1]*Department of Materials and Ceramic Engineering, Centre for Research in Ceramics and Composite Materials, CICECO, University of Aveiro, 3810 193 Aveiro, Portugal*
[2]*Institut für Struktur und Funktionskeramik, Montanuniversitaet Leoben, Peter Tunner Straße 5, A 8700 Leoben, Austria*
[3]*Materials Center Leoben Forschung GmbH, Roseggerstraße 12, A 8700 Leoben, Austria*

(Received 13 November 2013; accepted 11 December 2013; published online 7 January 2014)

A polarized Raman analysis of ferroelectric $(K_{0.5}Na_{0.5})NbO_3$ (KNN) single crystals is presented. The Raman modes of KNN single crystals are assigned to the monoclinic symmetry. Angular-dependent intensities of A′, A″, and mixed A′ + A″ phonons have been theoretically calculated and compared with the experimental data, allowing the precise determination of the Raman tensor coefficients for (non-leaking) modes in single-domain monoclinic KNN. This study is the basis for non-destructive assessments of domain distribution by Raman spectroscopy in KNN-based lead-free ferroelectrics.
[http://dx.doi.org/10.1063/1.4860416]

Ferroelectric $K_xNa_{1-x}NbO_3$ (KNN) system is a good candidate for lead-free sensor/actuator applications, owing to its comparable properties to lead zirconate titanate (PZT).[1] The piezoelectric constant (d_{33}) of doped KNN was reported to be higher than 300 pC/N, whereas with suitable texturing of the ceramic microstructure it was improved to 416 pC/N, thus comparable to soft PZT.[1] If not textured, KNN may show inferior electromechanical properties but it is still a viable replacement among other lead-free alternatives like barium titanate ($BaTiO_3$) and bismuth sodium titanate ($Bi_{0.5}Na_{0.5}TiO_3$), especially owing to its relatively high Curie temperature ($T_c \approx 420\,^{\circ}C$) and high radial coupling coefficient (48%).[2] Attempts to improve the electromechanical response of KNN have been reported using chemical substitutions,[1,3–5] sintering aids like $K_{5.4}CuTa_{10}O_{29}$ (KCT) and CuO,[3,6] and by controlling the poling process.[7] Since KNN lacks a morphotropic phase boundary (MPB the base of high performance in PZT[9–13]), a convenient strategy to enhance the extrinsic piezoelectricity of KNN ceramics is by texturing the microstructure.[1,8]

KNN is a solid solution between $KNbO_3$ and $NaNbO_3$, where studies have shown that the optimal piezoelectric properties appear when the K/Na ratio is 1:1 on the A-site of the ABO_3 perovskite.[2,9,14] The crystallographic structure of KNN was first proposed by Shirane *et al.* as orthorhombic at room temperature, which changes to tetragonal at ∼200 °C and then to cubic at ∼400 °C.[15] The orthorhombic assignment is also consistent with a monoclinic structure with $\beta > 90°$. Ahtee and Hewat[16] refined the neutron diffraction data of KNN compositions corresponding to $x = 0.02$ and 0.1 and proposed the monoclinic symmetry as more adequate. The monoclinic phase was reported from the refinement of cell parameters in nanosized pulverized KNN ceramics[17,18] and conventionally prepared ceramics.[19] Since the difference between the orthorhombic and monoclinic structures is very small, many researchers used the orthorhombic phase for the refinement of the cell parameters of KNN at room temperature from X-ray diffraction (XRD)[20] and neutron data.[21] Therefore, a lack of consensus regarding the structure of KNN exists and clarification is required. In addition, since the crystal symmetry influences the domain configuration, which affects the electro-mechanical properties of KNN and hence practical applications, it is important to have a technique for domain analysis that relates domain configuration with crystal symmetry details. Among the existing techniques to visualize domains, piezoresponse force microscopy (PFM) and Raman spectroscopy have been preferred in recent years for domain visualization in piezoceramics.[22–27] The information provided from both techniques is complementary and, when combined, allows greater insight into the domain structure. Domain imaging by PFM is based on the principle of the converse piezoelectric effect, where an alternating current (AC) bias is applied either to the probe tip or to the sample in order to excite deformation. PFM can be used to image and manipulate ferroelectric domains but it is restricted to the surface of the material (in nanometer range). In contrast, most of the Raman intensity signal (which originates from the inelastic scattering of an incident monochromatic light wave) comes from deep inside the material (e.g., 10 μm in the present case). Indeed, surface domains may not represent domain configuration for the bulk due to surface effects. The distinction between surface and bulk domains may contribute to a better understanding and better design of the material. Although Raman spectroscopy cannot distinguish between 180° oriented domains, and thus cannot detect their polarization, it can obtain a domain orientation distribution function (ODF) from in-plane rotation measurements under fixed light polarization.[28–30] Building up an ODF by

a)Author to whom correspondence should be addressed. E mail: marco.deluca@mcl.at. Tel.: +43 3842 402 4113. Fax: +43 3842 402 4102.

Raman measurements in polycrystalline KNN requires obtaining reliable single crystal data, since the scattering efficiency depends on the unit-cell Raman tensor parameters.[31] Not much Raman spectroscopy data are available for the KNN system and more specifically for KNN single crystals. Published data on undoped KNN polycrystalline materials assigned the Raman modes based on the vibrations of groups of atoms,[17] without taking into account the symmetry. For doped KNN ceramics, the assignment was done with tetragonal[32] or orthorhombic/tetragonal[27] phases, but never taking into account the possibility of a monoclinic unit cell.

The present study aims to clarify KNN crystal structure by combining XRD and Raman measurements. In particular, a precise Raman mode assignment is performed according to group theory and to the angular dependence of Raman mode intensity, confirming that the structure is monoclinic. The dependence of Raman modes (A′, A″, and mixed A′+A″) on crystal rotation is measured, and theoretical predictions are compared with the experimentally observed phonon intensity changes, thus allowing the precise retrieval of Raman tensor coefficients for all (non-leaking) investigated modes.

KNN single crystals were prepared by a self-flux method. High purity chemical reagents of K_2CO_3 (Merck, purity $\geq 99\%$), Na_2CO_3 (Chempur, $\geq 99.5\%$), Nb_2O_5 (Chempur, 99.9%), and B_2O_3 (Merck, 95%) were used as starting powders to prepare KNN single crystals. The size of the as-grown crystals varies between $2 \times 2 \times 0.5$ mm and $8 \times 3 \times 3$ mm. Further details on the preparation method have been reported elsewhere.[33] The XRD pattern obtained from KNN single crystals is reported in the inset of Fig. 1(a); X-ray studies were performed using a SIEMENS D500 (Cu Kα radiation; $\lambda = 0.15418$ nm) diffractometer with graphite monochromator. Rietveld refinement was done with fullprof® software and XRD peaks were indexed as belonging to the monoclinic space group (*Pm*). The calculated unit cell parameters of monoclinic KNN crystals are a = 3.9997 Å, b = 3.9478 Å, c = 3.9981 Å with $\beta = 90°\ 22'$.[34]

Raman spectroscopy experiments were performed with a Raman microprobe (LabRAM HR 800, Horiba Jobin Yvon, Villeneuve d'Ascq, France) with single monochromator. The 514.55 nm laser excitation was employed in the backscattered configuration with a lateral spatial resolution of 1 μm (Long-working distance 100× objective, numerical aperture (NA) = 0.8, Olympus, Tokyo, Japan). This spot size enabled us the laser excitation to be focused within a single domain of the KNN crystal, as confirmed by PFM analyses on the same

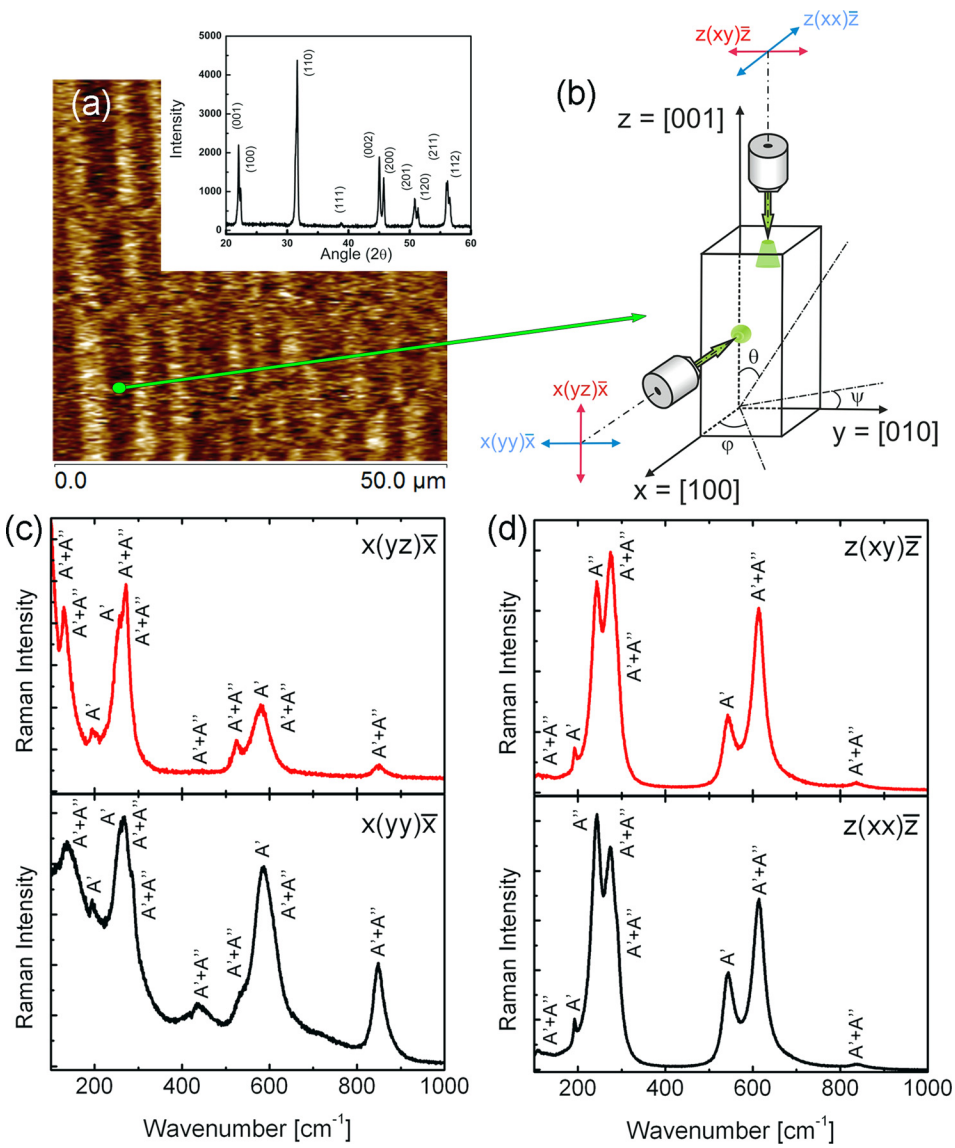

FIG. 1. (a) PFM image recorded on the (001) plane of the KNN single crystal.[33] The green spot has the dimensions of the Raman lateral resolution (~1 μm); the Raman spot is contained within one single domain (average domain width: 2.6 μm). Inset: XRD pattern of milled powder of KNN single crystals prepared by the self flux method. (b) Schematic of the polarization settings used in our Raman experiments. Light was propagated along either the [001] or the [100] directions of the monoclinic KNN crystal. Sample rotation was performed either on the [001] or the [100] axes and the position of the crystal with respect to the laser polarization vectors was expressed in terms of the Euler angles. (c) and (d) Raman spectra of monoclinic KNN obtained on the (100) and (001) planes, respectively, for both the cross and parallel polarized configurations. The assignment of Raman modes is reported in the figure.

crystal[33] (cf., Fig. 1(a), Multimode, NanoScope IIIA, Veeco instruments); the system is equipped with external lock-in amplifier (SR-830, Stanford Research), function generator (FG120, Yokogawa), and voltage amplifier (7602, Krohn-Hite). A conductive probe (PPP-NCHR Nanosensors, Switzerland length: 125 μm, thickness: 4.0 μm, width: 30 μm, resonance frequency: 355 kHz, and spring constant: 50 N/m) was used. The domain length was found to vary between 6.5 μm and 12 μm, and the average domain width is 2.6 μm.[33] Spectra were collected in the following polarized configurations (in Porto notation[35]): $x(yy)x$, $x(yz)x$, $z(xx)z$, and $z(xy)z$, where $x = [100]$, $y = [010]$, and $z = [001]$ with respect to the principal axes of the perovskite unit cell (cf., schematic in Fig. 1(b)). Rotation experiments were performed either on the (001) or the (100) planes of the KNN crystal with the aid of a rotating microscope table eucentric with the optical axis of the microscope (rotation angles defined in terms of the Euler angles, cf., Fig. 1(b)). Spectral fitting was performed with commercially available software (LABSPEC 4.02, Horiba Jobin Yvon) using Gaussian/Lorentzian functions.

If lattice disorder is not taken into account, group theory predicts 33 Raman-active modes for the monoclinic *Pm* phase ($\Gamma_{\mathrm{Raman,Pm}} = 22\mathrm{A}' + 11\mathrm{A}''$) and 24 Raman-active modes for the orthorhombic *Amm*2 phase ($\Gamma_{\mathrm{Raman,Amm2}} = 8\mathrm{A}_1 + \mathrm{A}_2 + 7\mathrm{B}_1 + 8\mathrm{B}_2$).[36] All of these modes, except the A_2 in the *Amm*2 symmetry, are also IR active and thus are split into their longitudinal (LO) and transverse (TO) optical components. Many of the modes are not observable due to the selection rules relaxation caused by the disorder on the A-site; hence the assignment of Raman spectra to one of the two symmetries has to be done considering the angular dependence of the intensity of the observed modes. The scattering intensity dependence of a Raman mode is given by[31]

$$\mathrm{I_k} \propto |\mathrm{e_i}\Re_\mathrm{k}\mathrm{e_s}|^2, \tag{1}$$

where $\mathrm{e_i}$ and $\mathrm{e_s}$ are the polarization vectors of incident and scattered light, respectively, whereas $\Re_k$ is the Raman scattering tensor of the k-th mode. For the monoclinic *Pm* structure, these are given by

$$\Re_{\mathrm{A}'} = \begin{pmatrix} \mathrm{a} & 0 & \mathrm{d} \\ 0 & \mathrm{b} & 0 \\ \mathrm{d} & 0 & \mathrm{c} \end{pmatrix}, \quad \Re_{\mathrm{A}''} = \begin{pmatrix} 0 & \mathrm{e} & 0 \\ \mathrm{e} & 0 & \mathrm{f} \\ 0 & \mathrm{f} & 0 \end{pmatrix}. \tag{2}$$

In the orthorhombic *Amm*2 structure, by

$$\Re_{\mathrm{A_1}} = \begin{pmatrix} \mathrm{a} & 0 & 0 \\ 0 & \mathrm{b} & 0 \\ 0 & 0 & \mathrm{c} \end{pmatrix}, \quad \Re_{\mathrm{A_2}} = \begin{pmatrix} 0 & \mathrm{d} & 0 \\ \mathrm{d} & 0 & 0 \\ 0 & 0 & 0 \end{pmatrix},$$
$$\Re_{\mathrm{B_1}} = \begin{pmatrix} 0 & 0 & \mathrm{e} \\ 0 & 0 & 0 \\ \mathrm{e} & 0 & 0 \end{pmatrix}, \quad \Re_{\mathrm{B_2}} = \begin{pmatrix} 0 & 0 & 0 \\ 0 & 0 & \mathrm{f} \\ 0 & \mathrm{f} & 0 \end{pmatrix}. \tag{3}$$

The proportionality constant in Eq. (1) depends on the instrumentation; it is therefore convenient to normalize the Raman tensor parameters in (2) and (3). From a closer look to the Raman tensors in Eqs. (2) and (3), it can be noticed that in the case of a monoclinic phase A′ modes would be present in both *(yy)* and *(xx)* configurations and A″ modes in both *(yz)* and *(xy)* configurations. On the other hand, in an orthorhombic phase $\mathrm{A_1}$ modes would be present in both *(yy)* and *(xx)* configurations but in the *(yz)* and *(xy)* configurations only $\mathrm{B_1}$ and $\mathrm{A_2}$ modes could be Raman-active, respectively. Figs. 1(c) and 1(d) present the Raman spectra of a KNN single crystal collected in the $x(yz)x$, $x(yy)x$, $z(xy)z$, and $z(xx)z$ configurations [$x(yz)x$ and $x(yy)x$ on the (100) plane, $z(xy)z$ and $z(xx)z$ on the (001) plane].[34] It can clearly be seen that the number of observed Raman modes is lower than predicted by group theory for both structures, with the exception of the *(xy)* configuration (for which in the case of an orthorhombic structure only the $\mathrm{A_2}$ mode should be visible). The higher number of observed modes is a clear indication that the symmetry is lower than *Amm*2. We have modeled the angular dependence of the intensity for each mode observed in the spectra for all polarization configurations, considering the Raman tensors for both the *Pm* and the *Amm*2 phases, and the *Pm* case gave always the best fit. The intensity dependence was modeled with Mathematica 9 (Wolfram Research, Inc., Champaign, IL) using Eqs. (1) (3) and expressing the Raman tensors in terms of the Euler angles. For the

TABLE I. Raman mode assignment for monoclinic KNN. For each mode, the selection rules for (001) and (100) planes, and the mode symmetry are reported. Normalized Raman tensor parameters resulting from the best fit procedure are also shown. The position of modes observed by other authors in KNN and simi lar systems (NN NaNbO$_3$) is reported.

	Plane			Raman tensor parameters						
Mode [cm ^{1}]	(001)	(100)	Type	a	b	c	e	KNN [cm ^{1}][45]	NN [cm ^{1}][40]	PZT [cm ^{1}][37,39]
105	X	X	A′+A″	…	…	…	…	151	153	150
130	X	X	A′+A″	…	…	…	…	177	175	…
192	X	X	A′	…	…	…	…	200	201	200 205
243	X		A′	…	0.93	1	…	224	218	220 230
256		X	A′+A″	0.59	…	1	0.12	248	247	252 260
272	X	X	A′+A″	…	…	…	…	280	276	280 295
288	X	X	A′+A″	…	…	…	…	…	…	…
436		X	A′+A″	1	…	0.49	0.14	431	435	…
525		X	A′+A″	…	…	…	…	…	…	510
545	X		A′	…	0.94	1	…	…	…	…
576		X	A′	0.67	…	1	…	572	557	…
613	X	X	A′+A″	…	…	…	…	611	602	600
840	X	X	A′+A″	…	…	…	…	872	867	748

monoclinic structure, A′ modes generally possess 180° periodicity for parallel polarized configurations and 90° periodicity for the cross-polarized ones. A″ modes possess 90° periodicity in both cases, whereas A′ and A″ mode mixing would produce the same periodicity as A′ but with a phase shift. Both pure and mixed modes were tested in our model, and it was determined that in most of the cases a mixture of A′ and A″ modes was the best combination. Mode mixing in the monoclinic structure commonly occurs in perovskites, e.g., morphotropic PZT.[37–39] The assignment resulting from this fitting procedure is indicated for the Raman modes in Figs. 1(c) and 1(d) and is summarized in Table I along with the results from previous authors.

Fig. 2 reports the angular dependence of selected Raman modes of the investigated KNN single crystals in all investigated polarization configurations (blue = parallel; red = cross). Some of the modes (cf., Figs. 2(a) and 2(b) the mode at 105 cm ^{1} and Figs. 2(c) and 2(d) the mode at 272 cm ^{1}) were visible on both the (001) and (100) planes, while other modes only appear on one plane [Fig. 2(e), mode at 243 cm ^{1} (001); Fig. 2(f), mode at 256 cm ^{1} (100); Fig. 2(g), mode at 545 cm ^{1} (001) and Fig. 2(h), mode at 576 cm ^{1} (100)]. The solid curves in Figure 2 result from the best fit procedure obtained from Eqs. (1) and (2); with the assumption of the crystal being a single monoclinic domain within the investigated laser volume. This is motivated by the fact that the lateral size of the laser spot (∼1 μm) is consistently smaller than the average domain width, thus confirming that we were able to position the laser spot within one domain (cf., Fig. 1(a)). In addition, from the PFM response we concluded that the domain walls are perpendicular to the surface. Considering that 90% of the observed intensity comes from about 10 μm in-depth of the KNN crystal (as determined by defocusing experiments,[34,41–44]) the observed Raman

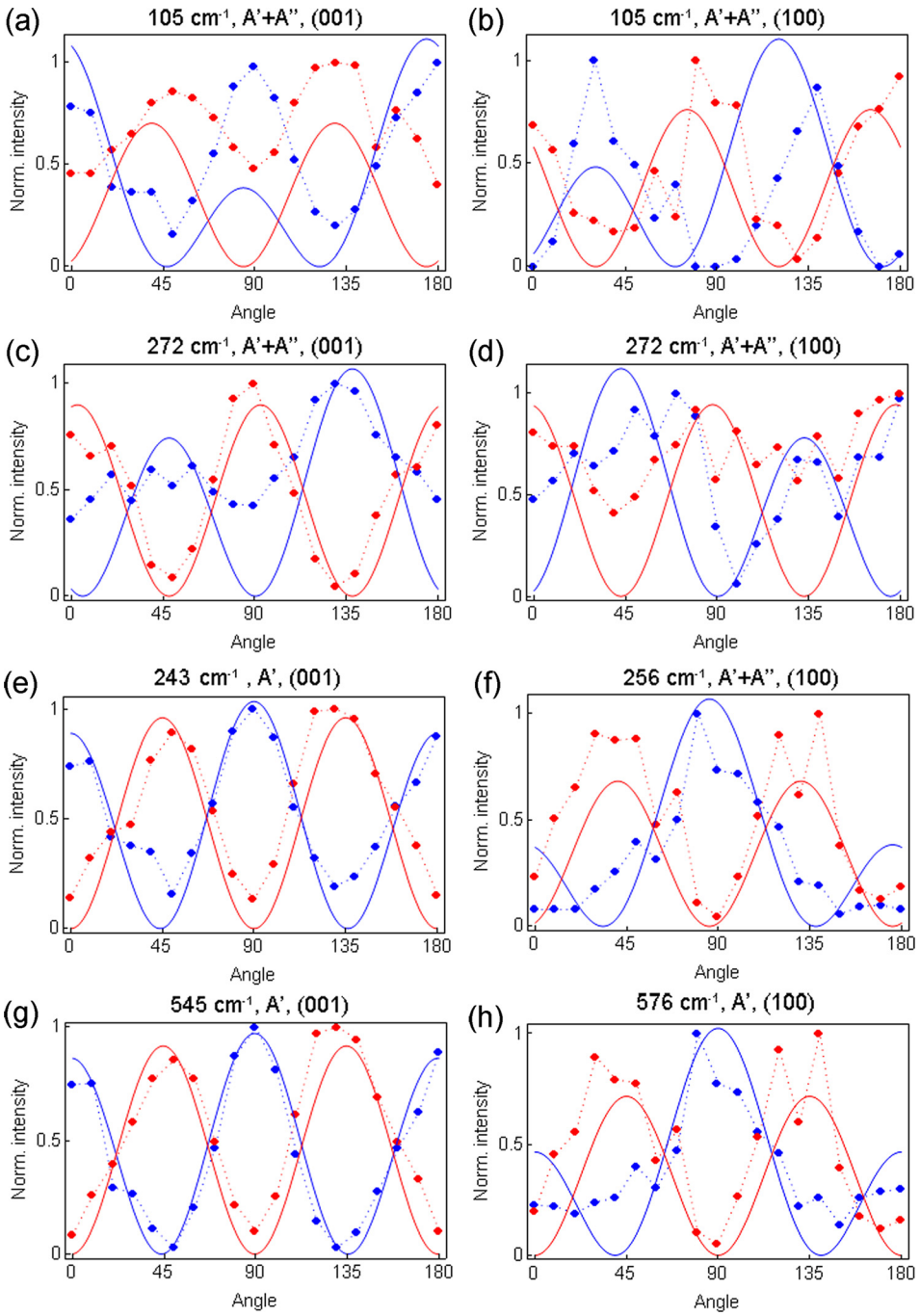

FIG. 2. Angular intensity dependence of selected Raman modes of the monoclinic KNN crystal. The position of the mode, its symmetry, and the plane on which it was retrieved are indicated on the graphs. The solid curves represent the best fitting procedure with Eqs. (1) and (2) (transformed in terms of the Euler angles), allowing retrieval of the Raman tensor parameters for the modes in (e) (h). Blue parallel polarized; red cross polarized.

signal should originate from only one ferroelectric domain. From Fig. 2, however, it is evident that only modes that were observed either on the (001) or the (100) plane (Figs. 2(e) 2(h)) were very well represented by our model. For modes visible on both (001) and (100) planes (Figs. 2(a) 2(d)), a significant leakage was present in either the cross or the parallel signal. It is well-known that even in cases in which the Raman spot is positioned on a single domain, the use of high-NA objectives could produce depolarization effects.[46] Given our use of a NA = 0.8 objective, we interpret the observed leakage as due to the effect of neighboring domains contributing to the Raman signal. Interestingly, this happens only when the considered Raman mode appeared on both the (001) and the (100) plane. This depends on the relative value of the Raman tensor parameters for those modes; we have calculated the Raman response for pure A′ and A″, and for mixed modes and concluded that modes appearing on either the (001) or the (100) plane have only partially-filled Raman tensors. This makes them less sensitive to contributions from diversely-oriented neighboring domain states, and are thus the most reliable ones. The values of the Raman tensor parameters we report for these modes, can be freely used as single-domain input parameters for quantitative analyses of domain distributions in KNN single and polycrystalline materials. The retrieval of the Raman tensor parameters for all Raman modes of KNN is possible only if a single-crystal single-domain KNN is used. We are now in the process of producing a crystal with these characteristics and this remains a topic for a future work.

In summary, a polarized Raman analysis was performed on KNN single crystals. By rotating KNN crystals, using a eucentric fixture under fixed polarized light, and positioning the laser spot on single domains of sufficient size, we were able to perform a precise Raman mode assignment for the monoclinic structure. In addition, we obtained the Raman tensor parameters for modes appearing either on (001) or (100) planes of the crystal, thus opening the way to quantitative analyses of domain distribution in KNN materials.

The work was supported by the Federal Ministry for Transport, Innovation and Technology (bmvit) and Austrian Science Fund (FWF): TRP 302-N20. Collaboration within COST Action MP0904 SIMUFER was also gratefully acknowledged. The authors would like to thank DI Stefan Strobl (Materials Center Leoben Forschung GmbH) for the help in the interpretation of defocusing experiments in KNN. Dr. Katharina Resch and DI Katharina Bruckmoser (Lehrstuhl für Werkstoffkunde und Prüfung der Kunststoffe, Montanuniversitaet Leoben) are gratefully acknowledged for supporting the Raman experiments at the Department of Kunststofftechnik of the Montanuniversitaet Leoben. Muhammad Asif Rafiq, E. Costa, and P. M. Vilarinho acknowledge FEDER, QREN, COMPETE, CICECO, and FCT. Muhammad Asif Rafiq acknowledges FCT for the financial support under the scholarship, SFRH/BD/66942/2009.

[1]Y. Saito, H. Takao, T. Tani, T. Nonoyama, K. Takatori, T. Homma, T. Nagaya, and M. Nakamura, Nature **432**, 84 (2004).
[2]R. E. Jaeger and L. Egerton, J. Am. Ceram. Soc. **45**, 209 (1962).
[3]M. Matsubara, T. Yamaguchi, W. Sakamoto, K. Kikuta, T. Yogo, and S. Hirano, J. Am. Ceram. Soc. **88**, 1190 (2005).
[4]Y. Saito and H. Takao, Ferroelectrics **338**, 17 (2006).
[5]C. W. Ahn, C. H. Choi, H. Y. Park, S. Nahm, and S. Priya, J. Mater. Sci. **43**, 6784 (2008).
[6]M. Matsubara, K. Kikuta, and S. Hirano, J. Appl. Phys. **97**, 114105 (2005).
[7]F. Rubio Marcos, J. J. Romero, D. A. Ochoa, J. E. Garcia, R. Perez, and J. F. Fernandez, J. Am. Ceram. Soc. **93**, 318 (2010).
[8]K. Wang and J. F. Li, Adv. Funct. Mater. **20**, 1924 (2010).
[9]B. Jaffe, W. R. Cook, and H. Jaffe, *Piezoelectric Ceramics* (Academic Press, London, 1971), Vol. 3.
[10]F. Huaxiang and R. E. Cohen, Nature **403**, 281 (2000).
[11]B. Noheda, J. A. Gonzalo, L. E. Cross, R. Guo, S. E. Park, D. E. Cox, and G. Shirane, Phys. Rev. B **61**, 8687 (2000).
[12]B. Noheda, D. E. Cox, G. Shirane, R. Guo, B. Jones, and L. E. Cross, Phys. Rev. B **63**, 014103 (2000).
[13]R. Guo, L. E. Cross, S. E. Park, B. Noheda, D. E. Cox, and G. Shirane, Phys. Rev. Lett. **84**, 5423 (2000).
[14]M. Ahtee and A. M. Glazer, Acta Crystallogr. A **32**, 434 (1976).
[15]G. Shirane, R. Newnham, and R. Pepensky, Phys. Rev. **96**, 581 (1954).
[16]M. Ahtee and A. W. Hewat, Acta Crystallogr. A **31**, 846 (1975).
[17]Y. Shiratori, A. Magrez, and C. Pithan, J. Eur. Ceram. Soc. **25**, 2075 (2005).
[18]Y. Shiratori, A. Magrez, and C. Pithan, Chem. Phys. Lett. **391**, 288 (2004).
[19]J. Tellier, B. Malic, B. Dkhil, D. Jenko, J. Cilensek, and M. Kosec, Solid State Sci. **11**, 320 (2009).
[20]H. E. Mgbemere, R. P. Herber, and G. A. Schneider, J. Eur. Ceram. Soc. **29**, 1729 (2009).
[21]H. E. Mgbemere, M. Hinterstein, and G. A. Schneider, J. Eur. Ceram. Soc. **32**, 4341 (2012).
[22]M. Deluca, T. Sakashita, C. Galassi, and G. Pezzotti, J. Eur. Ceram. Soc. **26**, 2337 (2006).
[23]S. Pojprapai, J. L. Jones, and M. Hoffman, Appl. Phys. Lett. **88**, 162903 (2006).
[24]M. Deluca, T. Sakashita, and G. Pezzotti, Appl. Phys. Lett. **90**, 051919 (2007).
[25]M. Deluca, M. Higashino, and G. Pezzotti, Appl. Phys. Lett. **91**, 091906 (2007).
[26]L. J. Hu, Y. H. Chang, M. L. Hu, M. W. Chang, and W. S. Tse, J. Raman Spectrosc. **22**, 333 (1991).
[27]W. Zhu, J. Zhu, M. Wang, B. Zhu, X. Zhu, and G. Pezzotti, J. Raman Spectrosc. **43**, 1320 (2012).
[28]M. Pigeon, R. E. Prudhomme, and M. Pezolet, Macromolecules **24**, 5687 (1991).
[29]R. Perez, S. Banda, and Z. Ounaies, J. Appl. Phys. **103**, 074302 (2008).
[30]K. Okai, W. Zhu, and G. Pezzotti, Phys. Status Solidi A **208**, 1733 (2011).
[31]R. Loudon, Adv. Phys. **13**, 423 (1964).
[32]F. Rubio Marcos, M. A. Banares, J. J. Romero, and J. F. Fernandez, J. Raman Spectrosc. **42**, 639 (2011).
[33]M. A. Rafiq, M. E. V. Costa, and P. M. Vilarinho, "Establishing the do main structure of $(K_{0.5}Na_{0.5})NbO_3$ (KNN) single crystals by piezoforce response microscopy," Sci. Adv. Mater. (in press).
[34]See supplementary material at http://dx.doi.org/10.1063/1.4860416 for more details on the XRD study (including fit parameters, atomic positions, and a fitted XRD pattern), the angular variation of the Raman spectra in all configurations, and the determination of the investigated probe dimensions.
[35]T. C. Damen, S. P. S. Porto, and B. Tell, Phys. Rev. **142**, 570 (1966).
[36]E. Kroumova, M. I. Aroyo, J. M. Perez Mato, A. Kirov, C. Capillas, S. Ivantchev, and H. Wondratschek, Phase Transitions. **76**, 155 (2003).
[37]K. C. V. Lima, A. G. Souza Filho, A. P. Ayala, J. Mendes Filho, P. T. C. Freire, F. E. A. Melo, E. B. Araújo, and J. A. Eiras, Phys. Rev. B **63**, 184105 (2001).
[38]A. G. Souza Filho, K. C. V. Lima, A. P. Ayala, I. Guedes, P. T. C. Freire, F. E. A. Melo, J. Mendes Filho, E. B. Araújo, and J. A. Eiras, Phys. Rev. B **66**, 132107 (2002).
[39]M. Deluca, H. Fukumura, N. Tonari, C. Capiani, N. Hasuike, K. Kisoda, C. Galassi, and H. Harima, J. Raman Spectrosc. **42**, 488 (2011).
[40]Z. X. Shen, X. B. Wang, M. H. Kuok, and S. H. Tang, J. Raman Spectrosc. **29**, 379 (1998).
[41]D. M. Lipkin and D. R. Clarke, J. Appl. Phys. **77**, 1855 (1995).
[42]A. Atkinson, S. C. Jain, and S. J. Webb, Semicond. Sci. Technol. **14**, 561 (1999).
[43]S. Guo and R. I. Todd, J. Eur. Ceram. Soc. **30**, 641 (2010).
[44]V. Presser, M. Keuper, C. Berthold, and K. G. Nickel, Appl. Spectrosc. **63**, 1288 (2009).
[45]Z. Wang, H. Gu, Y. Hu, K. Yang, M. Hu, D. Zhou, and J. Guan, Cryst. Eng. Comm. **12**, 3157 (2010).
[46]G. Tarrach, L. P. Lagos, Z. R. Hermans, and F. Schlaphof, Appl. Phys. Lett. **79**, 3152 (2001).